Journal of Low Temperature Physics manuscript No.
(will be inserted by the editor)

J. Egger[1] · **E. Krotscheck**[1,2] · **R. E. Zillich**[1]

Bose and Fermi gases with Lennard-Jones interactions

XX.XX.2011

Keywords Bose Gas, Fermi Gas, equation of state, scattering length
Abstract We study a model for cold Bose and Fermi gases based on the Lennard-Jones interaction, using the optimized (Fermi-)hypernetted-chain ((F)HNC-EL) method. For comparison, we also have carried out path integral ground state Monte Carlo (PIGSMC) simulations in the Bose case. By varying the density and the coupling strength for the Lennard-Jones potential, we cover the whole range of dilute, weakly interacting gases up to the dense, strongly interacting case of liquid ^{3}He and ^{4}He. Below about 20 percent helium equilibrium density, the simplest version of the (F)HNC-EL theory is accurate within better than 1 percent.

PACS numbers: 74.70.Tx,74.25.Ha,75.20.Hr

1 Introduction

The Lennard-Jones interaction

$$V_{\rm LJ} = 4\varepsilon\left[\left(\frac{\sigma}{r}\right)^{12} - \left(\frac{\sigma}{r}\right)^{6}\right] \tag{1}$$

has for decades provided a useful model for examining interacting gases, liquids, and solids. It can be tuned from a rather weak to a strong interaction and shows the essential phase transitions of a quantum liquid, namely the liquid-gas and the liquid-solid transition. In the appropriate parameter range, the Lennard-Jones liquid can also be considered a model system for cold molecular gases.

The energy scale of the interaction is characterized by ε and the length scale by σ. As a convention, we measure energies in units of $\hbar^2/2m\sigma^2$, and length in

[1]Institute for Theoretical Physics, Johannes Kepler University, Linz, Austria
[2]Department of Physics, University at Buffalo, SUNY Buffalo NY 14260,USA
E-mail: eckhard.krotscheck@jku.at

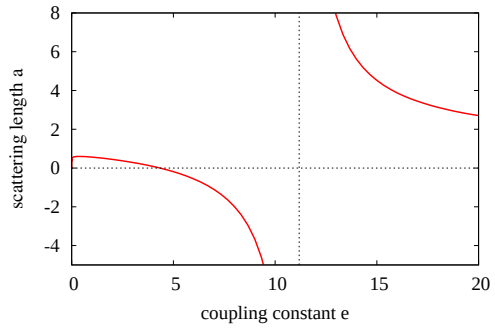

Fig. 1 The plot shows the scattering length a as a function of the coupling constant e. The vertical line at $e = 11.18$ indicates the coupling strength where a two-body bound state appears.

units of σ. The Hamiltonian is then given by

$$H = -\sum_i \nabla_i^2 + \sum_{i<j} v(|\mathbf{x}_i - \mathbf{x}_j|) \tag{2}$$

where $\mathbf{x}_i = \mathbf{r}_i/\sigma$ are the dimensionless coordinates and $v(x) = 4e\left[x^{-12} - x^{-6}\right]$. $e = 2m\sigma^2\varepsilon/\hbar^2$ is the dimensionless coupling constant. In this work we tune e and the dimensionless density ρ to investigate different regimes of correlation strength.

In cold gas applications, the interaction is often characterized by its scattering length a because this is, in the low density limit, the only quantity that determines the equation of state, see *e.g.* Ref. [1]. The scattering length is determined by the coupling constant e. Fig. 1 shows the relationship in the regime $1 < e < 20$. For large e, the potential provides a reasonable model of the interaction between two helium atoms[2]: ^{3}He corresponds to $e = 8.26$ whereas ^{4}He corresponds to $e = 11.02$. The Lennard-Jones model predicts the observed[3,4,5] weakly bound state of ^{4}He dimers for coupling strengths $e > 11.18$, corresponding to a well depth of $10.37\,K$

Over the past three decades, a set of "generic" equations has been derived that contain the essential physics of the many-body problem. We shall spell out these equations further below. The first derivation was based on the optimization of the Jastrow-Feenberg form of the wave function[6], however, it was noted very early[7] that "...it appears that the optimized Jastrow function is capable of summing all rings and ladders, and partially all other diagrams, to infinite order." The observation was quantified by Jackson *et. al.* who showed that the same equations can be derived by self-consistently summing ring- and ladder diagrams of the perturbation series[8,9,10]. Further derivations of the same equations have been done within the coupled-cluster theory[11] and within a pair-density functional approach[12]. Thus, we have at hand a system of generic equations, termed hypernetted chain - Euler Lagrange equations, that determine the ground state structure of a quantum fluid.

Since the analogy between different formulations of the many body problem has been worked out in much less detail for fermions, we will base our discussion on the Jastrow-Feenberg theory for strongly interacting systems. The method starts

with an *ansatz* for the wave function[6]

$$\Psi_0(1,\ldots,N) = F(\mathbf{r}_1,\ldots,\mathbf{r}_N)\Phi_0(1,\ldots,N)$$
$$F(\mathbf{r}_1,\ldots,\mathbf{r}_N) = \exp\frac{1}{2}\left[\sum_i u_1(\mathbf{r}_i) + \sum_{i<j} u_2(\mathbf{r}_i,\mathbf{r}_j) + \ldots\right], \tag{3}$$

where $\Phi_0(1,\ldots,N)$ is a model state, normally a Slater-determinant for fermions and $\Phi_0(1,\ldots,N) = 1$ for bosons. An index i denotes both spatial and spin coordinates. The correlations $u_n(\mathbf{r}_1,\ldots,\mathbf{r}_n)$ are obtained by minimizing the energy

$$\frac{\delta}{\delta u_n(\mathbf{r}_1,\ldots,\mathbf{r}_n)} \frac{\langle\Psi_0|H|\Psi_0\rangle}{\langle\Psi_0 \mid \Psi_0\rangle} = 0\,. \tag{4}$$

In an approximate evaluation of the energy expectation value, it is important to make sure that the resulting equations are consistent with the *exact* variational determination of the correlations. It has turned out that the hypernetted chain hierarchy of approximations is the only systematic approximation scheme that preserves the properties of the variational problem[6]. This hierarchy is also the one that allows the diagrammatic identification of Jastrow-Feenberg theory and Feynman-diagram based perturbation theories[8,9,10].

2 Bosons

2.1 Generic Many-Body Equations

In what follows, it is convenient to define the Fourier transform with a density factor, *i.e.* $\tilde{f}(k) \equiv \rho \int d^3r\, e^{i\mathbf{r}\cdot\mathbf{k}} f(r)$. The equations are formulated in terms of the pair distribution function $g(r)$ and the static structure function

$$S(k) = 1 + \rho \int d^3r\, e^{i\mathbf{r}\cdot\mathbf{k}} [g(r) - 1]\,. \tag{5}$$

There are two equivalent forms of the HNC-EL equations. The first one is a "Bogoliubov" form

$$S(k) = \left[1 + \frac{4m}{\hbar^2 k^2}\tilde{V}_{\mathrm{p-h}}(k)\right]^{-\frac{1}{2}}. \tag{6}$$

that determines $S(k)$ as a function of a "particle-hole interaction"

$$V_{\mathrm{p-h}}(r) = g(r)\,[v(r) + V_{\mathrm{I}}(r)] + \frac{\hbar^2}{m}\left|\nabla\sqrt{g(r)}\right|^2 + [g(r) - 1]\,w(r)\,. \tag{7}$$

Above, we have introduced the "induced interaction"

$$\tilde{w}(k) = -\frac{\hbar^2 k^2}{4m}\left[1 - \frac{1}{S^2(k)}\right][2S(k) + 1] \tag{8}$$

and an "irreducible" part of the interaction, $V_{\mathrm{I}}(r)$, see below.

The second formulation of the same equation is a Bethe-Goldstone equation for the square-root of the pair distribution function $g(r)$

$$\frac{\hbar^2}{m}\nabla^2\sqrt{g(r)} = [v(r)+w(r)+V_{\rm I}(r)]\sqrt{g(r)}\,. \tag{9}$$

Eq. (9) has the form of a 2-body Schrödinger for the zero-energy scattering wave function. Since $g(r)$ has to fulfill $g(r)\sim 1+\mathscr{O}(r^{-4})$ for $r\to\infty$, $w(r)$ and $V_I(r)$ must guarantee that the s-wave scattering length of the "in medium" interaction potential $v(r)+w(r)+V_{\rm I}(r)$ is always zero. In either form, the HNC-EL equations are nonlinear and can be solved iteratively to obtain $g(r)$.

The energy per particle has the form

$$E = E_{\rm R}+E_{\rm Q}+E_{\rm I} \tag{10}$$

where

$$E_{\rm R} = \frac{\rho}{2}\int d^3r\left[g(r)v(r)+\frac{\hbar^2}{m}\left|\nabla\sqrt{g(r)}\right|^2\right] \tag{11}$$

and

$$E_{\rm Q} = -\int\frac{d^3k}{(2\pi)^3\rho}\frac{\hbar^2k^2}{8m}\frac{(S(k)-1)^3}{S(k)}\,. \tag{12}$$

Eqs. (6) or (9) follow by minimizing this energy expression with respect to $g(r)$. $E_{\rm I}$ is a functional of the pair distribution function, it generates the irreducible interaction through

$$V_{\rm I}(r) = \frac{2}{\rho}\frac{\delta E_{\rm I}}{\delta g(r)}\,. \tag{13}$$

$E_{\rm I}$ is, within the Jastrow-Feenberg variational theory, expressible in terms of elementary diagrams and multiparticle correlations. In parquet-diagram theory it is a sum of diagrams that is neither particle-particle nor particle-hole reducible [13]. Taking into account three particle correlations and elementary diagrams with up to five nodes leads to the HNC-EL/5+T method, while the simplest HNC-EL version is obtained by completely omitting $V_{\rm I}(r)$. This defines the HNC-EL/0 approximation. HNC-EL/5+T contains one phenomenological parameter that accounts for the slow convergence of the series of elementary diagrams [12].

2.2 Path Integral Ground State Monte Carlo

Path integral ground state Monte Carlo (PIGSMC) [14] takes advantage of the equivalence between the Schrödinger equation in imaginary time and a diffusion equation, similar to diffusion Monte Carlo. A trial state Ψ_G is propagated in imaginary time towards the ground state wave function Φ_0

$$\Psi(R,\beta) = e^{-\beta H}\Psi_G(R) \longrightarrow e^{-E_0\beta}\Phi_0(R) \text{ for } \beta\to\infty \tag{14}$$

where $R=(\mathbf{r}_1,\ldots,\mathbf{r}_N)$ is the set of coordinates of N particles. In order to evaluate the evolution operator $e^{-\beta H}$, it is factorized into a product of short-time evolution

operators, $e^{-\beta H} = (e^{-\Delta\tau H})^M$, where $\Delta\tau = \beta/M$. This allows the use of short-time approximations for $e^{-\Delta\tau H}$. Therefore, like in path integral Monte Carlo, we perform Metropolis sampling of a whole "evolution path" of configurations $(R_0,\ldots,R_{2M})$, where R_i is now the set of $3N$ coordinates of all particles at discrete time steps $\tau_i = i\Delta\tau$. In PIGSMC, the end of the paths of length β are weighted by the trial state Ψ_G from which the time evolution starts and which guides the random walk. The middle of the path, at time step $\tau_M = \beta/2$, corresponds to a state $\Psi(R,\tau_M)$ evolved for a time span $\beta/2$. For sufficiently large $\beta/2$, according to Eq. (14), $\Psi(R,\tau_M)$ approximates the exact ground state, $\Psi(R,\frac{\beta}{2}) \to \Phi_0(R)$. In PIGSMC the following distribution function is sampled by a Metropolis random walk

$$\rho(R_0,\ldots,R_{2M}) = \Psi_G(R_0)\prod_{j=1}^{2M} G(R_{j-1},R_j,\Delta\tau)\,\Psi_G(R_{2M})\,. \qquad (15)$$

Here G is the coordinate representation of the evolution operator in imaginary time $e^{-\Delta\tau H}$. We use a short-time approximation which is based on a multi-product expansion of $G(R_{j-1},R_j,\Delta\tau)$ up to any desired order in $\Delta\tau$.[15] In practice, we found that for ^{4}He the fourth-order scheme offers the best trade-off between numerical complexity and efficiency. Therefore the fourth-order multi-product expansion is used here. All simulations were done with 256 particles in a cubic simulation box of side length $L = (N/\rho)^{1/3}$, with periodic boundary conditions.

2.3 Numerical Analysis

Since both ^{4}He and ^{3}He undergo spinodal decomposition at about 75% of saturation density, the low-density limit can never be reached for He. By reducing the coupling constant e, we decrease the attraction of the LJ potential and thus prevent spinodal decomposition at lower densities. We can make, by comparison between HNC-EL/0, HNC-EL/5+T and PIGSMC, quantitative statements on the accuracy of the HNC-EL method.

The calculation of the equation of state of a strongly interacting Bose system is by now a routine matter. Fig. 2 shows the equation of state $E(\rho)/N$ for several coupling constants e, and compares with PIGSMC results. We show both the results of the simple HNC-EL/0 approximation as well as results of a full HNC-EL/5+T calculation. The HNC-EL calculations are orders of magnitude less costly computationally than PIGSMC simulations, but the agreement of the HNC-EL/5+T results with the PIGSMC results is excellent. The discrepancies with HNC-EL/0 increase with density. It is well known that HNC-EL/0 recovers only about 75% percent of the binding energy of ^{4}He at the experimental saturation density, and we obtain a similar result for $e = 10$.

Fig. 2 also shows that, for $e \gtrsim 5$, the equation of state ends at the spinodal point, *i.e.* the density ρ where the hydrodynamic speed of sound vanishes and the system becomes unstable against infinitesimal fluctuations. The spinodal point moves to smaller ρ as e is decreased, and for $e \lesssim 4$ and smaller there is no spinodal point anymore. Instead we find stable solutions down to arbitrarily low density. This low density regime will be discussed in detail in terms of the s-wave scattering length in the following section.

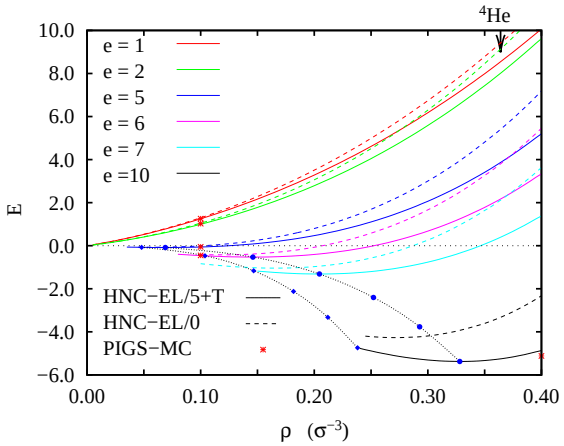

Fig. 2 (Color online) The figure shows the equation of state of the Lennard-Jones liquid in the strongly interacting regime as a function of coupling constant and density, obtained by HNC-EL/5+T (full lines) and HNC-EL/0 (dashed lines). Also shown are the spinodal points (blue diamonds connected by a dotted line), the equilibrium densities (blue circles connected by a dotted line) and PIGSMC data (red stars, error bars are smaller than the symbol size). The arrow at the top of the figure indicates the equivalent equilibrium density of ^{4}He.

Fig. 3 shows the static structure function $S(k)$ and the pair distribution function $g(r)$ for $e = 1,5$ at low density $\rho = 0.1$ and $e = 10$ at high density $\rho = 0.4$. In order to be compatible with the periodic boundary conditions, for the PIGSMC results for $S(k)$ we have to restrict the wave vectors to $\mathbf{k} = 2\pi(n_1, n_2, n_3)/L$, where n_i are integers. Again, the agreement between HNC-EL/5+T and PIGSMC is excellent, except for the low k limit of $S(k)$, especially in the case of low density, $\rho = 0.1$. The statistical error is much smaller than the difference between the HNC-EL/5+T and PIGSMC results. PIGSMC performs less satisfactorily for small k since it relies on the decay of the trial wave function towards the ground state. Long wave length phonons (i.e. with small k) decay slowest, and therefore, for finite decay time, the evolved trial state may still be contaminated with long wave length phonons, which leads to a bias in the low k behavior of $S(k)$. We note that the total energy per particle is much less affected by these residual contributions of low energy excitations. The problem could be rectified by longer decay times β (rendering the simulations more expensive) or better trial wave functions – such as the generalized Jastrow ansatz (3) optimized by the HNC-EL method itself. Instead, in the present work we employed the simple McMillan ansatz $\prod_{i<j} e^{-\alpha^5/|\mathbf{r}_i - \mathbf{r}_j|^5}$ for the trial wave function, where we optimzed α by variational Monte Carlo. The combination of HNC-EL and PIGSMC, with HNC-EL providing the trial wave function, will be a subject of future work.

2.4 Low density limit

Cold gases are only weakly correlated due to their low density, and thus do not require highly sophisticated many-body treatments appropriate for the helium liquids. The problem at hand is, due to the hard-core of the interaction, *a priori*

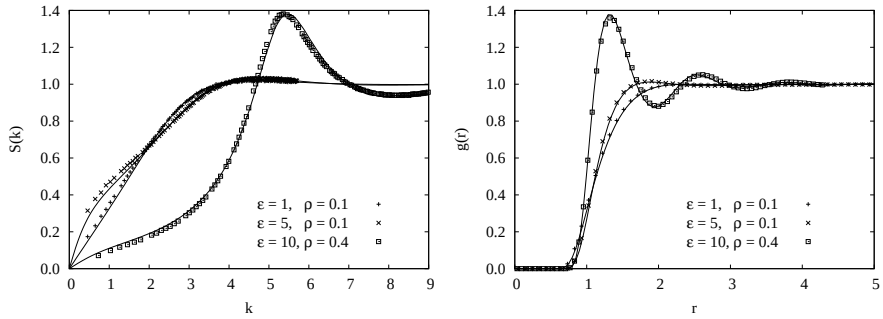

Fig. 3 The figure shows three representative calculations of the static structure function $S(k)$ (left) and the pair distribution function $g(r)$ (right) in PIGSMC (markers) and HNC-EL/5+T (solid line). The errorbars of the PIGSMC results are smaller than the size of the symbols.

not susceptible to a mean-field treatment. One deals with the hard core repulsion normally by constructing an equivalent soft-core effective interaction that is characterized by the scattering length. Microscopic many-body theory can deal with short-ranged repulsion directly. We demonstrate here how the low-density limit comes out directly from our manifestly microscopic theory.

Below about 25 percent of the ^{4}He saturation density, we can ignore $E_{\rm I}$ and $V_{\rm I}(r)$ because these go at least as ρ^3 or ρ^2, respectively. The term $E_{\rm Q}$ also goes as ρ^2, thus $E_{\rm R}$ is the only term that survives in the low-density limit. Minimizing $E_{\rm R}$ with respect to $\sqrt{g(r)}$ leads to Eq. (9) with $w(r) = V_{\rm I}(r) = 0$, *i.e.* it reduces to the zero-energy scattering equation

$$\frac{\hbar^2}{m}\nabla^2\sqrt{g(r)} = v(r)\sqrt{g(r)}\,. \tag{16}$$

The asymptotic form of the solution is

$$\sqrt{g(r)} \sim 1 - \frac{a}{r} \tag{17}$$

where a is the scattering length. Because of the long range of $\sqrt{g(r)}$ we must now be careful when using Eq. (16) for the calculation of $E_{\rm R}$:

$$\begin{aligned} E_{\rm R} &= 2\pi\rho\int dr r^2\left[g(r)v(r) + \frac{\hbar^2}{m}\left|\frac{d\sqrt{g(r)}}{dr}\right|^2\right] \\ &= 2\pi\rho\lim_{R\to\infty}\left[\int_{r<R} dr r^2\sqrt{g(r)}\left[v(r) - \frac{\hbar^2}{m}\nabla^2\right]\sqrt{g(r)} + \frac{\hbar^2}{m}R^2\frac{d\sqrt{g(R)}}{dR}\right] \\ &= \frac{2\pi\rho\hbar^2 a}{m}\,. \end{aligned} \tag{18}$$

That is, $E_{\rm R}$ recovers the low density limit[16] because the first integral in the second line vanishes as a consequence of the zero-energy scattering equation (16). We note that the limit $R\to\infty$ is not trivial, because for $R\to\infty$, $\sqrt{g(r)} \sim 1 - {\rm O}(r^{-4})$

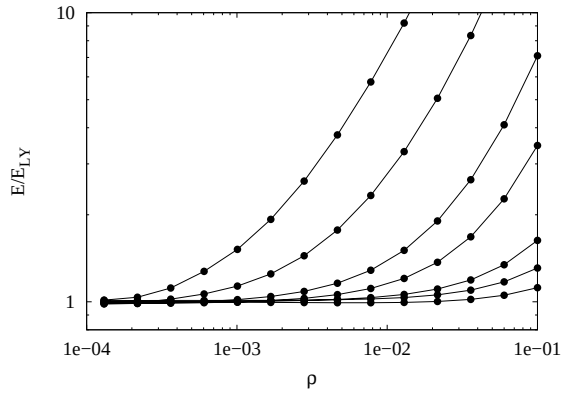

Fig. 4 Ratio of the energy obtained by HNC-EL/0 and the Lee-Yang expansion, Eq. (19), for coupling constants $e = 1, 2, 3, 4, 4.2, 4.3, 4.32$. Higher curves $E/E_{\rm LY}$ correspond to higher e, and thus to lower scattering length a, which changes sign at $e \approx 4.336$.

at finite density ρ. With decreasing ρ, the interparticle distance r where g crosses over from the regime where eq. (17) is valid to the regime where $1 - \mathrm{O}(r^{-4})$ is valid is pushed to larger and larger distances, as we have checked numerically.

The result is, *per se*, not surprising, the proper many-body treatment of the problem provides, while hardly more complicated than a mean field calculation, more information: Noting that $\tilde{V}_{\rm p-h}(0+) \to 2E_{\rm R}$ as $\rho \to 0$, Eq. (6) shows that $E_{\rm R} > 0$ and, hence $a > 0$ is a necessary condition for a stable ground state in the homogeneous low density limit.

The non-analyticity of the equation of state as a function of scattering length emerges from the square-root in the Bogoliubov equation (6) and leads to the well-known expansion of the equation of state for low density and small scattering length by Lee and Yang[17]

$$E_{\rm LY} = 4\pi \frac{\hbar^2 \rho a}{2m} \left[1 + \frac{128}{15\pi^{1/2}} \left(na^3 \right)^{1/2} + \ldots \right] . \tag{19}$$

In order to make quantitative statements about how the mean-field limit is approached, we discuss the equation of state as a function of the density and the *s*-wave scattering length a. It is sufficient to use the HNC-EL/0 approximation because elementary diagrams and triplet correlations are negligible at low density. In Fig. 4 we show the relative deviations of the energy obtained by HNC-EL from the Lee-Yang expansion (19). The relative deviations increase with an increase of the coupling constant e towards $e \approx 4.336$ where a vanishes, see Fig. 1. In other words, if we decrease a to a small but finite positive value, we have to go to exceedingly low densities to recover the regime where Eq. (19) is valid.

As we have mentioned at the end of the previous section, HNC-EL ceases to give low density solutions, if e is raised above a certain value and the absence of low density solutions means the system would undergo spinodal decomposition. As expected, spinodal decomposition appears right at $e \approx 4.336$, i.e. when a vanishes. For $e > 4.336$ and even for coupling strength e beyond the divergence of a, see Fig. 1, where bound two-body states appear, HNC-EL will yield solutions for the homogeneous ground state only if the density lies above the spinodal point. In this regime of large coupling strength the ground state is a self-bound (liquid or solid) state, not the gas state that is of interest in the field of ultra-cold gases. In

order to describe quantum gases of e.g. alkali atoms, which are only meta-stable and decay via three-body scattering, also HNC-EL will require the use of an effective potential obtained from low-energy scattering cross sections, or other means of stabilizing the meta-stable gas state.

We stress that, unlike mean field approximations, the HNC-EL method also provides a correct description of the stability. The input to the HNC-EL/0 equations is the LJ potential and nowhere in the equations appears the scattering length a. We only use a to discuss the results, but not to obtain the results.

3 Fermions

3.1 FHNC-EL Theory

In principle, the analogy between the fermion version of Jastrow-Feenberg theory, parquet-diagram theory, and coupled cluster theory persists for fermions. However, details have not been worked out to an extent that the basic equations of the fermion Jastrow-Feenberg theory have been derived by other means. The Fermi-HNC equations are, due to the multitude of exchange diagrams, also more complicated than the Bose-HNC equations. For a general discussion of the equations and the corresponding Euler equations, see Ref. [18].

The simplest version of the FHNC-EL theory ("FHNC-EL//0") is no more complicated than the HNC-EL method for bosons. The fermion version of the Bogoliubov equation (6) is

$$S(k) = \frac{S_{\rm F}(k)}{\sqrt{1+\dfrac{4mS_{\rm F}^2(k)}{\hbar^2k^2}\tilde{V}_{\rm p-h}(k)}}\,, \tag{20}$$

where $S_{\rm F}(k)$ is the static structure function of the free Fermi gas. The "induced interaction" is given by

$$\tilde{w}_{\rm I}(k) = -\frac{\hbar^2k^2}{2m}\left[\frac{1}{S_{\rm F}(k)}-\frac{1}{S(k)}\right]^2\left[2\frac{S(k)}{S_{\rm F}(k)}+1\right]. \tag{21}$$

A useful auxiliary quantity is the "direct-direct" correlation function $\Gamma_{\rm dd}(r)$, the Fourier transform of which is given by

$$\tilde{\Gamma}_{\rm dd}(k) = \big(S(k)-S_{\rm F}(k)\big)/S_{\rm F}^2(k)\,. \tag{22}$$

The pair distribution function $g(r)$ can be obtained from $\Gamma_{\rm dd}(r)$ as

$$g(r) = [1+\Gamma_{\rm dd}(r)][1+C(r)] \tag{23}$$

where, roughly speaking, $C(r)$ is related to exchange while $\Gamma_{\rm dd}(r)$ are the correlations due to the interaction. In general, they both depend on each other, and the FHNC equations cannot be solved for them separately. In the FHNC-EL//0 approximation, $[1+C(r)]$ is in leading order in the density equal to the pair distribution $g_F(r)$ of the free Fermi gas.

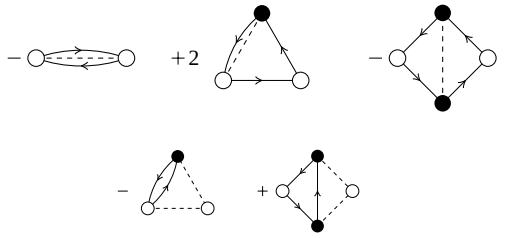

Fig. 5 The upper row of diagrams in the figure show the first non-trivial correction to the set of *ee* exchange diagrams. The diagrammatic conventions of Ref. 18 are used; the trivial diagram representing the exchange loop $S_F(k)-1$ is not shown. The lower row shows the leading contribution to $\tilde{X}_{\rm de}(k)$. The combinations of all diagrams shown in each row guarantee the long-wavelength properties eqns. (26) and (27).

In terms of these quantities, the total energy in FHNC-EL//0 approximation is

$$\begin{aligned} E &= T_{\rm F}+E_{\rm R}+E_{\rm Q}\,, \\ E_{\rm R} &= \frac{\rho}{2}\int d^3r\, g_F(r)\left[\left[1+\Gamma_{\rm dd}(r)\right]v(r)+\frac{\hbar^2}{m}\left|\nabla\sqrt{1+\Gamma_{\rm dd}(r)}\right|^2\right], \qquad (24) \\ E_{\rm Q} &= -\int\frac{d^3k}{(2\pi)^2\rho}\,\frac{\hbar^2k^2}{8m}\tilde{\Gamma}^2_{\rm dd}(q)\left[S^2_{\rm F}(q)/S(q)-1\right]. \end{aligned}$$

where $T_{\rm F}$ is the energy per particle of the free Fermi system. The similarity to Eqs. (6), (8), (11) and (12) is obvious.

More advanced versions of the theory include more complicated sets of exchange diagrams, either in an order-by-order expansion or in the form of integral equations [18]. The exact form of the structure function $S(k)$ in terms of "non-nodal" exchange diagrams is

$$S(k)=\frac{\left(1+\tilde{X}_{\rm ee}(k)\right)\left(1+\left(1+\tilde{X}_{\rm ee}(k)\right)\tilde{\Gamma}_{\rm dd}(k)\right)}{[1-\tilde{X}_{\rm de}(k)]^2}\,. \qquad (25)$$

The most important features that must be satisfied for a meaningful implementation of the optimization are the long-wavelength properties

$$\tilde{X}_{\rm ee}(k)=S_F(k)-1+\mathscr{O}(k^2)\quad\text{as}\quad k\to 0+ \qquad (26)$$
$$\tilde{X}_{\rm de}(k)=\mathscr{O}(k)\quad\text{as}\quad k\to 0+\,. \qquad (27)$$

The first non-trivial diagrams contributing to $\tilde{X}_{\rm ee}(k)$ and $\tilde{X}_{\rm de}(k)$ are shown in Fig. 5; the simplest approximation consistent with the variational problem is $\tilde{X}_{\rm ee}(k)=S_F(k)-1$ and $\tilde{X}_{\rm de}(k)=0$. We shall refer to the approximations including no diagrams (corresponding to simplest version of FHNC-EL introduced above), the $X_{\rm ee}$ diagrams, and the $X_{\rm de}$ diagrams shown in Fig. 5 as to FHNC-EL//0, FHNC-EL//1, and FHNC-EL//2, respectively. The implementation including "elementary diagrams" and triplet correlations as described in Ref. [18] will be referred to as FHNC-EL/5+T.

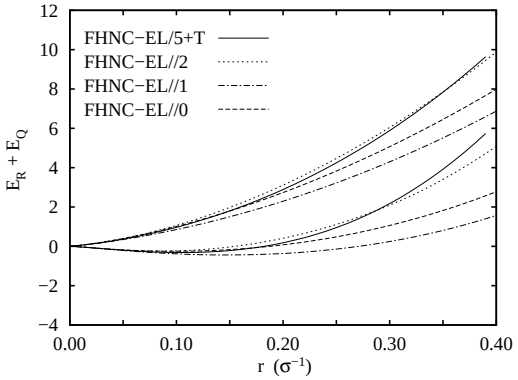

Fig. 6 The correlation energy $E_{\rm R} + E_{\rm Q}$ is shown as function of density for various levels of the FHNC-EL method, for coupling constants $e = 1$ (upper set of curves) and $e = 5$ (lower set of curves). CBF corrections as described in section 3.2 are included in all calculations.

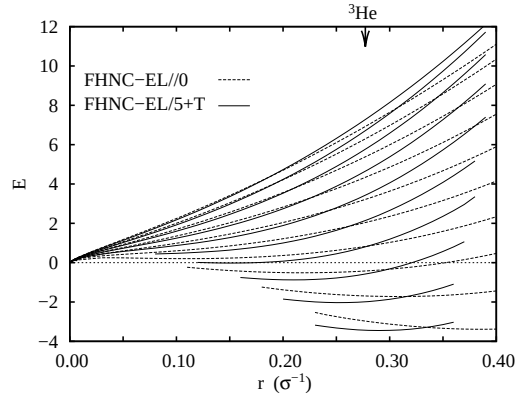

Fig. 7 The equation of state is shown in the regime of coupling constants $1 \leq e \leq 10$ (top curves to bottom curves). The FHNC-EL//0 approximation (dashed lines) is compared with the full FHNC-EL/5+T theory containing four- and five-body elementary diagrams and triplet correlations (full lines) as described in Ref. 18. The arrow points to the equilibrium density of ^{3}He.

A detailed numerical comparison between the different approximation levels of the FHNC-EL theory is tedious and not very illuminating. Fig. 6 shows two representative sets of calculations of the ground state energy, with energy of the free Fermi gas subtracted. Evidently, the overall convergence of the procedure is not as systematic as for bosons, the only clear message seems to be that both elementary diagrams and triplet correlations are important for saturation at high densities. In the low-density regime the message is similar to the one for bosons: The simplest version FHNC-EL//0 lies within a percent accuracy at densities of $0.05\ \sigma^{-3}$ and less. This is about 20 percent of the experimental saturation density of ^{3}He.

Fig. 7 shows the equation of state for coupling constants $1 \leq e \leq 10$ as calculated in the full FHNC-EL//5+T scheme described in Ref. [18] and in the simple FHNC//0 approximation (20)-(24). Note that in both figures 6 and 7 the correlated basis functions corrections described in the next section are also included.

3.2 Correlated Basis Functions (CBF)

Unlike for bosons, the Jastrow-Feenberg theory is not even in principle exact for fermions. This is a manifestation of the well-known “nodal surface” problem:

The nodes of the correlated wave function (3) are identical to those of the free Fermi gas. In Monte Carlo calculations, the problem can be cured by "releasing" the nodes, albeit at a high price in terms of computational cost. In semi-analytic theories like the Jastrow-Feenberg theory, one uses the correlation operator F to generate a complete basis of the Hilbert space,

$$\Psi_m(\mathbf{r}_1,\ldots,\mathbf{r}_N) = F(\mathbf{r}_1,\ldots,\mathbf{r}_N)\Phi_m(\mathbf{r}_1,\ldots,\mathbf{r}_N)\,. \tag{28}$$

The procedure has been implemented either as a finite-order perturbation expansion or by summing selected classes of diagrams, for a pedagogical review, see Ref. [19]. A working formula that sums all ring-diagrams in a correlated basis is

$$\frac{\Delta E_{RPA}}{N} = \frac{1}{2\rho}\Im m \int \frac{d^3k d\omega}{(2\pi)^4} \ln\left[\frac{1-\tilde{V}_{\rm p-h}(k)\chi_0(k,\omega)}{1-\tilde{V}_{\rm p-h}(k)\chi_0^{\rm MSA}(k,\omega)}\right]. \tag{29}$$

where $\chi_0(k,\omega)$ is the Lindhard function, and $\chi_0^{\rm MSA}(k,\omega)$ is the "collective approximation" for the Lindhard function,

$$\chi_0^{\rm MSA}(k,\omega) = \frac{\dfrac{\hbar^2k^2}{m}}{(\omega+i\eta)^2 - \left(\dfrac{\hbar^2k^2}{2mS_{\rm F}(k)}\right)^2}\,. \tag{30}$$

Note also that Eq. (20) follows from the RPA relationship

$$\begin{aligned} S(k) &= -\Im m \int_0^\infty \frac{d\omega}{\pi}\chi(k,\omega)\,, \\ \chi(k,\omega) &= \frac{\chi_0(k,\omega)}{1-\chi_0(k,\omega)\tilde{V}_{\rm p-h}(k)} \end{aligned} \tag{31}$$

if the Lindhard function is replaced by $\chi_0^{\rm MSA}(k,\omega)$.

These corrections are included in our numerical calculations. Their numerical effect is very small at low densities, it ranges from 0.2 to 0.4 $\hbar^2/2m\sigma^2$ at the highest density of $\rho = 0.4\sigma^{-3}$.

3.3 Low density limit

In the preceding analysis of Bose systems, we have shown how the low-density limit of the HNC-EL theory compares with the Lee-Yang expansion. In particular, we have been able to make quantitative statements on the density where mean field approximations are valid, and how well low-density expansions agree with manifestly microscopic calculations.

The situation is a bit more complicated for fermions. Basically, the analysis of section 2.4 is valid for fermions as well, however, the long range of the exchange corrections must be taken care of properly. It is still true that, after the kinetic energy T_F of the free Fermi gas, E_R is the leading term in the density expansion.

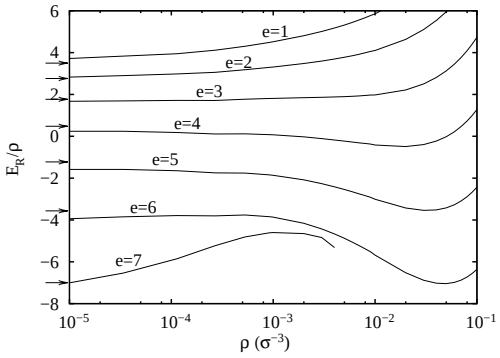

Fig. 8 The figure shows E_R/ρ in the limit of low densities for coupling constants $1 \leq e \leq 7$. The arrows in the left side show the theoretical limit $E_R/\rho = \pi\hbar^2 a/m$.

However, the factor $g_F(r)$ is, for $k_F \to 0$ $g_F(r) = 1 - \frac{1}{2}(rk_F)^2$, hence one would conclude

$$E_{\mathrm{R}} = \frac{\pi\rho\hbar^2 a}{m} + \mathscr{O}\left(k_F^{5/3}\right). \tag{32}$$

This assumes that the statistical correlations are much longer ranged than the dynamical correlations represented by $\Gamma_{\mathrm{dd}}(r)$. A second remark is concerned with the higher-order terms in k_F. Huang and Yang[16] prove that the equation of state has the low-density expansion (See also Ref. [1])

$$E = \frac{\hbar^2 k_F^2}{2m}\left[\frac{3}{5} + \frac{2}{3\pi}ak_F + \frac{4(11-2\ln 2)}{35\pi^2}(ak_F)^2 + \ldots\right] \tag{33}$$

The expansion (32) evidently misses the third term in Eq. (33). This is due to the fact that the Jastrow-Feenberg function approximates the exact particle-hole propagator by the "collective" Lindhard function (30). The problem can be cured by adding the perturbation corrections (29).

We note that, similar to the Bose case, the lowest order term gives a reasonably faithful approximation to the equation of state, whereas higher-order corrections are generally overshadowed by correlation effects.

Fig. 8 shows the low-density behavior of E_R/ρ for coupling constants between $e = 1$ and 7. Note that we had to go to a density an order of magnitude lower than in the Bose case to get reasonably close to that limit. The low-density limit has not been reached in our calculations, which indicates that correlation effects remain visible down to very low densities.

In Figs. 9 we show the direct correlation function $\Gamma_{\mathrm{dd}}(r)$ (the Fourier transformation of Eq. (22)) and the pair distribution function $g(r)$, Eq. (23), together with $g_F(r)$ of the free Fermi gas. The left panels show the results for a low density of $\rho = 4.22 \times 10^{-6}\sigma^{-3}$ for a range of coupling parameters between $e = 1$ (corresponding to a positive scattering length $a = 0.563\sigma$), and $e = 7$ (negative scattering length $a = -1.11\sigma$). In addition we show also $e = 4.336$ where $a = 0$. The direct correlations are of the range of the interaction, whereas exchange correlations become quite long ranged, with a characteristic length scale k_F^{-1}. When $a > 0$, the interaction is effectively repulsive and $g(r)$ is reduced with respect

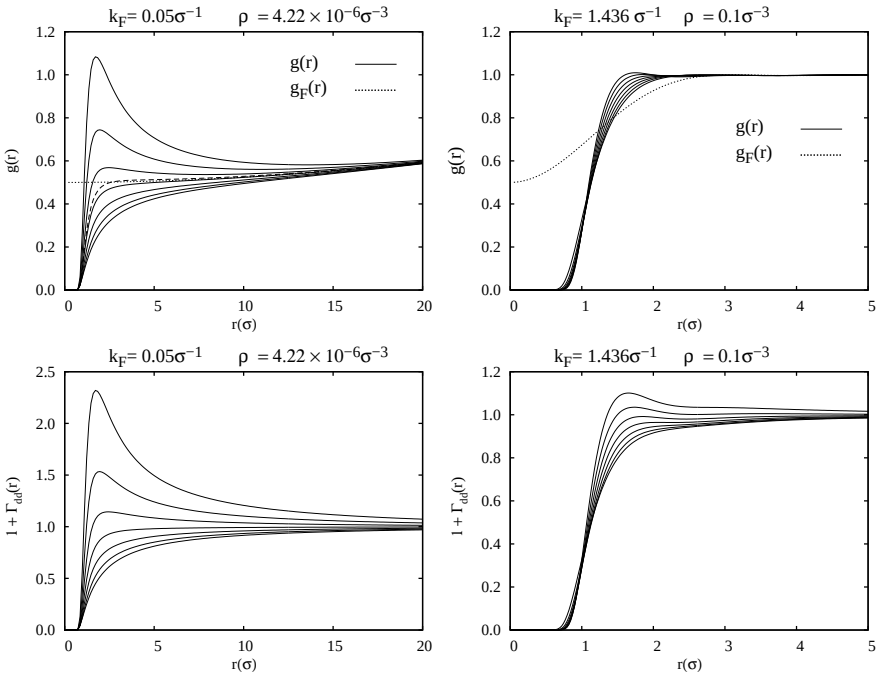

Fig. 9 The figures show the pair distribution function $g(r)$, the pair distribution function of the free Fermi gas $g_F(r)$, (upper panels), and the direct correlation function $1+\Gamma_{\rm dd}(r)$ (lower panels), for a density of $4.22\times10^{-6}\sigma^{-3}$ (left panels) and $0.1\sigma^{-3}$ (right panels). The coupling parameters $e=1\ \ldots,7$ correspond to scattering lengths $a=0.563\sigma,\ldots,-1.11\sigma$ respectively. Curves with higher nearest-neighbor peaks correspond to stronger coupling. The upper left panel also shows the pair distribution funtion for coupling strengths $e=4.366$ corresponding to zero scattering length (long dashed line). Note the different scales.

to $g_F(r)$. Conversely, $g(r)$ is enhanced with respect to $g_F(r)$ when $a<0$, corresponding to an effectively attractive interaction. In fact, in the $a<0$ regime where the system is stabilized only by the Pauli pressure, the direct correlation function develops an enormous peak, in particular at low densities. For $a=0$, we find that $g(r)$ follows indeed $g_F(r)$ most closely, except for very small $r\sim\sigma$, i.e. when two particles see the *real* repulsive part of the LJ interaction.

The right panels of Fig. 9 shows $\Gamma_{\rm dd}(r)$, $g(r)$ and $g_F(r)$ for the much higher density $\rho=0.1\sigma^{-3}$. There, the $g(r)$ is clearly dominated by the repulsive interaction of the LJ potential, and always far from $g_F(r)$. There are small fermionic exchange corrections, but there is no clear distinction of exchange and direct correlations.

3.4 Stability

A gas or liquid becomes unstable when the incompressibility vanishes. This indicates *generally* the spinodal point. In low density Bose gases the statement is equivalent to the statement that the scattering length goes through zero. At that

point, the HNC-EL equations cease to have solutions. The situation is similar in a Fermi fluid, but the Pauli pressure permits stable solutions also for interactions with a negative long-wavelength limit. From the expansion (33) one concludes that, in the low density limit [1]

$$mc^2 = \frac{\hbar^2 k_F^2}{3m}\left[1+\frac{2ak_F}{\pi}\right] \tag{34}$$

which sets a stability limit $ak_F > -\pi/2$.

An accurate numerical verification of the low density equation of state is difficult. It has been shown [20] that the long-wavelength limit of the particle-hole interaction is given by, provided all diagrams are included,

$$\tilde{V}_{\mathrm{p-h}}(0+) = m(c^2 - c_F^2) \tag{35}$$

where c is the hydrodynamic speed of sound, and c_F is the speed of sound of the non-interacting Fermi gas. The condition that the term under square-root of Eq. (20) be positive amounts to the stability condition $mc_F^2 + \frac{4}{3}\tilde{V}_{\mathrm{p-h}}(0+) > 0$ which is obviously incorrect. The problem can be cured by using Eq. (31) instead of (20) for calculating $S(k)$.

To get the correct density expansion of $\tilde{V}_{\mathrm{p-h}}(0+)$ it is necessary to include the three diagrams shown in the upper row of Fig. 5. Then, the leading term is

$$\tilde{V}_{\mathrm{p-h}}(0+) = \rho\int d^3r\left[1-\frac{1}{2}j_0^2(rk_F)\right]\left[\left[1+\Gamma_{\mathrm{dd}}(r)\right]v(r)+\frac{\hbar^2}{m}\left|\nabla\sqrt{1+\Gamma_{\mathrm{dd}}(r)}\right|^2\right] \tag{36}$$

which agrees, in leading order in k_F, with the hydrodynamic speed of sound obtained from E_R. The simple FHNC//0 approximation omits exchange terms in the particle-hole interaction and therefore the low-density limit of $\tilde{V}_{\mathrm{p-h}}(0+)$ misses a factor of 1/2. We note that it is exceedingly difficult to reach this limit numerically because $1+\Gamma_{\mathrm{dd}}(r)$ starts to develop an enormous peak at short distances, see Fig. 9.

All the aforementioned corrections are small, especially in the low-density regime of interest here. They contribute, however, to some numerical inaccuracies which prevent us from making statements of comparable precision as those made above for bosons.

4 Summary

We have carried out a comprehensive array of (F)HNC-EL calculations for quantum fluids and gases, from very low densities up to densities corresponding the the helium saturation density. We have shown that the (F)HNC-EL reproduces the exact low-density limits, and we have made quantitative statements on the density regime where low density expansions are valid. In general we found that the simplest (F)HNC-EL approximation is adequate up to 20 to 30 percent of the saturation density of the corresponding (Bose or Fermi) helium system. The convergence of the fermion expansion is somewhat slower, which is due to the multitude of exchange diagrams.

We have compared our Bose results with PIGSMC calculations and found excellent agreement for energy, pair distribution function, and static structure function with the simplest approximation (HNC-EL/0) for the energy at low density and with the best approximation (HNC-EL/5+T). This is expected since even the simplest HNC-EL/0 method contains all the relevant physics which is achieved by a consistent treatment of short- and long ranged correlations. For fermions, there are no Monte Carlo calculations to compare with, we could only assess the convergence of our calculations by examining different levels of implementation of FHNC-EL.

A very interesting regime is the range of coupling constants e where the associated s-wave scattering length a changes sign. For $a < 0$, HNC-EL correctly predicts that a Bose gas is unstable, but a Fermi gas is stabilized by the Pauli pressure. While for $a > 0$, the Fermi pair distribution g is suppressed to values below the free Fermi pair distribution, in the regime of $a < 0$ the interaction is effectively attractive and indeed we find that the Fermi pair distribution develops an enormous peak as we increase e. In other words short-ranged correlations *increase* as a becomes more negative. Similar findings for $a < 0$ were obtained by Astrakharchik et al.[21], who reported a peak in the pair correlation for antiparallel spins using diffusion Monte Carlo with a BCS trial wave function.

In the weakly interacting limit, the Fermi system can undergo a phase transition to a superfluid state[1]. CBF theory can be used to deal with that situation as well[19]. The correlation operator F can be used to generate a basis of spatially correlated BCS states; effectively, CBF theory provides a vehicle to generate weak, effective potentials from strong, bare potentials. Although the effective interaction entering the gap-equation is not identical to the particle-hole interaction (it is particle-hole reducible whereas $V_{\mathrm{p-h}}(r)$ is particle-hole irreducible), they agree in leading orders in a density expansion. Thus, one would expect that the system undergoes BCS pairing in the density regime of *positive compressibility* and *negative scattering length*.

Acknowledgements This work was supported, in part, by the Austrian Science Fund FWF under grants P21264 (to EK) and P23535 (to REZ)

References

1. L. D. Landau and E. M. Lifshitz, *Statistical Physics*, Course of Theoretical Physics, Vol. V (Pergamon Press Ltd., London - Paris, 1958).
2. J. de Boer and A. Michels, Physica **6**, 945 (1938).
3. F. Luo, G. C. Mc Bane, G. Kim, C. F. Giese, and W. R. Gentry, J. Chem. Phys. **98**, 3564 (1993).
4. F. Luo, C. F. Giese, and W. R. Gentry, J. Chem. Phys. **104**, 1151 (1996).
5. W. Schöllkopf and J. P. Toennies, J. Chem. Phys. **104**, 1155 (1996).
6. E. Feenberg, *Theory of Quantum Fluids* (Academic, New York, 1969).
7. H. K. Sim, C.-W. Woo, and J. R. Buchler, Phys. Rev. A **2**, 2024 (1970).
8. A. D. Jackson, A. Lande, and R. A. Smith, Physics Reports **86**, 55 (1982).
9. A. D. Jackson, A. Lande, and R. A. Smith, Phys. Rev. Lett. **54**, 1469 (1985).
10. E. Krotscheck, R. A. Smith, and A. D. Jackson, Phys. Rev. A **33**, 3535 (1986).

11. R. F. Bishop, in *Condensed Matter Theories*, Vol. 10, edited by M. Casas, J. Navarro, and A. Polls (Nova Science Publishers, Commack, New York, 1995) pp. 483–508.
12. C. E. Campbell, R. Folk, and E. Krotscheck, J. Low Temp. Phys. **105**, 13 (1996).
13. A. D. Jackson, A. Lande, R. W. Guitink, and R. A. Smith, Phys. Rev. B **31**, 403 (1985).
14. A. Sarsa, K. Schmidt, and W. Magro, J. Chem. Phys. **113**, 1366 (2000).
15. R. E. Zillich, J. M. Mayrhofer, and S. A. Chin, J. Chem. Phys. **132**, 044103 (2010).
16. K. Huang and C. N. Yang, Phys. Rev. **105**, 767 (1957).
17. T. D. Lee and C. N. Yang, Phys. Rev. **105**, 1119 (1957).
18. E. Krotscheck, J. Low Temp. Phys. **119**, 103 (2000).
19. E. Krotscheck, in *Introduction to Modern Methods of Quantum Many–Body Theory and their Applications*, Advances in Quantum Many–Body Theory, Vol. 7, edited by A. Fabrocini, S. Fantoni, and E. Krotscheck (World Scientific, Singapore, 2002) pp. 267–330.
20. E. Krotscheck, Phys. Rev. A **15**, 397 (1977).
21. G. E. Astrakharchik, J. Boronat, J. Casulleras, and S. Giorgini, Phys. Rev. Lett. **93**, 200404 (2004).